

# Structural Study of the Incorporation of Heavy Metals into Solid Phase Formed during the Oxidation of EDTA by Permanganate at High pH

GREGORY V. KORSHIN,<sup>\*,†</sup>  
HYUN-SHIK CHANG,<sup>†</sup>  
ANATOLY I. FRENKEL,<sup>‡</sup> AND  
JOHN F. FERGUSON<sup>†</sup>

Department of Civil and Environmental Engineering, Box 352700, University of Washington, Seattle, Washington 98115-2700, and Physics Department, Yeshiva University, 245 Lexington Avenue, New York, New York 10016

Properties of solid phases formed during the oxidation of EDTA by permanganate in a high-pH, high-ionic strength solution, and the retention of Cu<sup>2+</sup>, Ni<sup>2+</sup>, and Zn<sup>2+</sup> by them were examined. Morphologically, the solids were agglomerates of particles with sizes <100 nm. X-ray absorption spectroscopy (XAS) analysis indicated that these particles were birnessite. Its precipitation was accompanied by the removal of Zn<sup>2+</sup> and Cu<sup>2+</sup> released as a result of the breakdown of their complexes with EDTA. However, Ni<sup>2+</sup> was not removed from the supernatant. Cu<sup>2+</sup> was strongly bound by birnessite and exhibited little mobility in the pH range from 3 to 14. Zn<sup>2+</sup> was more mobile, especially at pH > 12. XAS showed that Cu<sup>2+</sup> binding sites were located within MnO<sub>6</sub> octahedra-comprised sheets that constitute birnessite while Zn<sup>2+</sup> was positioned between them.

## Introduction

Permanganate has been successfully used for in situ degradation of many organic contaminants (1, 2). At Hanford Nuclear Reservation in the state of Washington, it has been utilized to treat high pH, high ionic strength nuclear tank wastes that contain EDTA, NTA, and related ligands. These ligands are oxidized by alkaline permanganate to predominantly CO<sub>2</sub>, ammonia, and oxalic acid (1, 3, 4). Following the oxidation, complexes of these ligands with metal cations break down to release uncomplexed metal ions that precipitate, coprecipitate with, or adsorb on solids formed as a result of the reduction of permanganate. This improves the separation of the target elements (transuranic elements, TRU, and Sr<sup>90</sup>) that must be achieved during the treatment (3–6).

Solids formed by the reduction of permanganate at high pH play a crucial role in the removal of TRU and metals present in the wastes. Their nature has not been ascertained, although it has been observed that when the high-pH reduction of permanganate proceeds via the oxidation of H<sub>2</sub>O<sub>2</sub> and formate, the reaction yields the mixed Mn(IV) oxide birnessite that belongs to the phyllosulfate group (7). The paucity of information about manganese solids formed in situ in the important case of the permanganate treatment

of EDTA-containing nuclear wastes is in contrast with extensive studies of Mn oxides formed ex situ (8–15). These studies have shown that in birnessite and other phyllosulfates the MnO<sub>6</sub> units are arranged in two-dimensional sheets (11–15), whose local structure can be altered by metal cations (Cu<sup>2+</sup>, Ni<sup>2+</sup>, and Zn<sup>2+</sup>) incorporated into them (11, 13).

One practically important question is whether the in situ formed manganese solids bind TRU and other metal cations structurally and thus make them mobilization-resistant as long as the solid substrate remains structurally intact, or are the retained metals sorbed on the surface and can be mobilized without affecting the substrate, for instance, by acidic solutions or in the presence of complexing agents.

To address the above issues, we carried out experiments designed to ascertain the structural properties of solids precipitated during the permanganate oxidation of simulated wastes similar to those in Hanford tanks. EDTA was used as a representative chelating agent that was oxidized by MnO<sub>4</sub><sup>-</sup>. Cu<sup>2+</sup>, Zn<sup>2+</sup>, and Ni<sup>2+</sup> were chosen as target metals with which to quantify the incorporation of cations present in the wastes into the solid substrate. The structural data were obtained primarily using X-ray absorption spectroscopy (XAS).

## Experimental Section

All experiments were conducted at 20 °C using 50 mL polyethylene centrifuge tubes. The concentration of NaOH in the samples was 1 M (pH 14). The ionic strength was adjusted to 1.38 M with NaClO<sub>4</sub>. The initial concentration of EDTA in the solutions was 0.02 M, while that of the metal ions (Cu<sup>2+</sup>, Zn<sup>2+</sup>, and Ni<sup>2+</sup>) was 0.002 M. All chemicals were ACS reagent grade. Reagent water was obtained with a Millipore Super-Q water system. The amount of permanganate added to the solutions corresponded to MnO<sub>4</sub><sup>-</sup>/EDTA molar ratios of 1 and 4. Reactions between EDTA and permanganate caused manganese solids to form immediately, but the reaction was allowed to proceed for 40 h, long after the permanganate was completely consumed. The test tubes were mildly agitated during that time. The precipitated solids and supernatant were separated by centrifugation. Aliquots of the supernatant were collected to determine the concentration of target elements (Mn, Ni, Cu, and Zn) in them.

The separated solids were split into three subsamples that were washed at three constant pH values (3, 7, and 14, respectively) using two cycles of resuspension in the washing solutions (Milli-Q water with a desired pH) followed by centrifugation. The washed solids were retained on 0.45 μm filters, dried in a desiccator, and used in XAS measurements. Experiments were also carried out with the solids that were first resuspended at pH 14, and then the pH of the system was decreased gradually (with pH increments of 0.3–0.5 units) by adding HClO<sub>4</sub>. The supernatant was analyzed for Mn, Cu, Zn, and Ni to determine the influence of pH on the mobilization of the retained metal cations.

Concentrations of metals were measured with a Jobin-Yvon JY-138 Ultratrace inductively coupled plasma (ICP) atomic emission spectrometer. Prior to ICP analysis, all samples were filtered through a 0.45 μm filter and acidified with HNO<sub>3</sub>. For structural studies, dried solids were coated with carbon and their morphology was examined with a JEOL JSM-7000F scanning electron microscope (SEM). Brunauer-Emmett-Teller (BET) specific surface areas were determined using a Micromeritics Flow Sorb II 2300 instrument. A Philips PW 1820 X-ray diffractometer was employed to examine the

\* Corresponding author phone: (206)543-2394; fax: (206)685-9185; e-mail: Korshin@u.washington.edu.

<sup>†</sup> University of Washington.

<sup>‡</sup> Yeshiva University.

structural identities of the solids. XRD diffractograms were obtained using Cu/K $\alpha_1$  radiation (wavelength of 1.54059 Å).

XAS measurements were conducted in the transmission and fluorescence modes for Mn and Cu/Zn, respectively, at beam line X-18B, National Synchrotron Light Source (NSLS) at Brookhaven National Laboratory (BNL), Upton, NY. The X-ray energy was varied from 200 eV below to 1000 eV above the absorption K-edges of Mn, Cu, Zn, and Ni using a double crystal Si(111) monochromator. X-ray absorption near-edge structure (XANES) and extended X-ray absorption fine structure (EXAFS) data were obtained using 30% (for Mn) and 20% (for Ni, Cu, and Zn) detuning of the monochromator crystals. Because of the presence of a strong background from the manganese, a 13-element Ge fluorescence detector cooled with liquid nitrogen was used to detect the XAS signal of copper and zinc. For XAS measurements, the dried solid samples were deposited on an adhesive tape by brushing. The tape was folded several times to obtain sufficiently intense XAS signal. To process EXAFS data, Athena, Artemis, and FEFF6 programs were used (16). EXAFS data analysis was performed by nonlinear least-square fitting using theoretical EXAFS signal calculated with FEFF6 program. The optimization of EXAFS data fitting was based on the minimization of the corresponding  $\chi^2$  and maximization of  $R^2$  values, visual inspection of the data, and verification of the compatibility of the model assumptions and predictions with results of preceding research.

## Results and Discussion

Measurements of Mn concentrations in the supernatant in contact with the solids formed during the oxidation of EDTA by MnO $_4^-$  showed that all the manganese introduced as permanganate was incorporated into them. The surface area of the solids changed only slightly as the reduction of MnO $_4^-$  progressed, having values of 10.3 and 13.5 m $^2$ /g for reaction times 0.5 and 24 h (Figure S1, Supporting Information). SEM examination showed that the solids lacked specific morphological features and were aggregates with apparent sizes <100 nm. The presence of particles with sizes <10 nm was also notable (Figure S2, Supporting Information). Unambiguously identifiable narrow peaks were absent in the XRD diffractograms, although the location of the features located in the range of  $2\theta$  values 32–42° and 60–70° was close to that of XRD peaks of birnessite prepared ex situ. This observation was in agreement with the data of prior research (7, 17). The most prominent maximum in the diffractogram obtained for our samples was located at  $2\theta$  of 36.445°. This  $2\theta$  value corresponded to the spacing of 2.463 Å. This is very close to one of the characteristic spacings reported for several phyllosulfates including birnessite (2.470 Å), chalcophanite (2.460 Å), and todorokite (2.453 Å) (18, 19). However, the absence of an entire sequence of XRD peaks characteristic of crystalline birnessite (caused by the extremely small sizes of the particles formed via the reduction of permanganate by EDTA) required that other techniques of structural identification of the solids be used.

Their structure was explored based on the data from XAS. Prior research has indicated that XANES features of Mn in the pre-edge region and the position of its main 1s  $\rightarrow$  4p transition are sensitive to the oxidation state of Mn (20–23). Accordingly, K-edge Mn XANES data (Figure S3, Supporting Information) were examined to determine the oxidation state of Mn in the particles. Mn XANES spectra of particles formed at pH 14 and washed at pH 7 and 3 were identical to those shown in Figure S3 and also model compounds such as  $\delta$ -MnO $_2$  and birnessite (7, 24). This indicated that the dominant oxidation state of the manganese in the solids was Mn(IV). The lack of sensitivity of the features of the Mn K-edge XANES spectra to variations of the MnO $_4^-$ /EDTA molar ratio and pH of washing solutions indicated that the oxidation

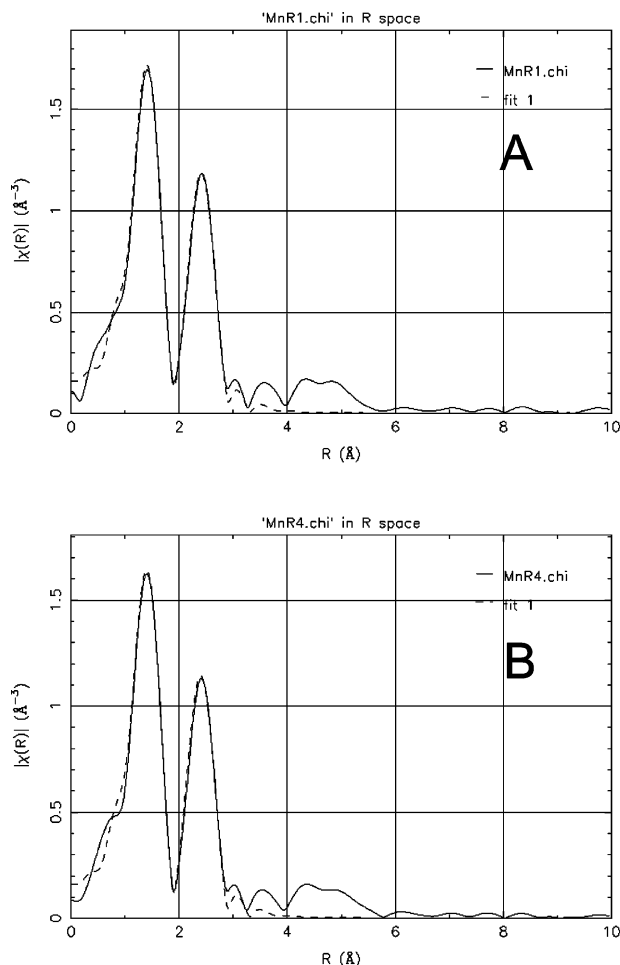


**FIGURE 1.** Mn radial density functions and fitting results for manganese solids formed at pH 14 and MnO $_4^-$ /EDTA molar ratios 1 (A) and 4 (B).

state of Mn in the particles remains constant in these conditions.

Fourier transform magnitudes of EXAFS (also known as EXAFS radial distribution functions, ERDFs) were calculated using the K-edge Mn EXAFS for the solids formed in situ at pH 14 (Figure 1). The peak positions in the ERDFs are not corrected for photoelectron phase shifts and, therefore, are shifted by ca. 0.5 Å toward the absorber relative to the actual interatomic distances. EXAFS data for the samples washed at pH 7.0 and 3.0 were indistinguishable from those represented in Figure 1. The first intense peak in the ERDF spectra is located at 1.40 Å. It corresponds to six oxygen atoms that comprise the inner complexation shell of the manganese. The second peak located at 2.41 Å corresponds to the second neighboring manganese atoms, and the small peak at 3.05 Å is likely to be associated with corner-sharing MnO $_6$  octahedra in birnessite (22, 25).

Mn–O and Mn–Mn distances that were determined via fitting of the experimental K-edge Mn EXAFS data are compiled in Table 1. In agreement with prior research, the coordination numbers for Mn–O and Mn–Mn bonds in these calculations were fixed as 6 (13–15, 20–22). The Mn–O (1.90  $\pm$  0.01 Å) and Mn–Mn distances (2.85  $\pm$  0.01 Å) in both samples were identical. The  $\sigma^2$  values for the Mn–O and Mn–Mn distances were small (for instance, 0.0057 and 0.0091 Å $^2$ , respectively, for particles generated at a 4.0 MnO $_4^-$ /EDTA ratio). This indicates that, despite the lack of the long-term order in the solids, they are highly ordered microstructurally. The Mn–Mn distance of 2.85 Å determined for our samples corresponds to the edge-sharing hexagonal octahedron

**TABLE 1. Structural Characteristics of Manganese in Solids Obtained by Oxidation of EDTA by Permanganate at pH 14<sup>a</sup>**

	Mn–O		Mn–Mn	
	<i>R</i> (Å)	$\sigma^2$ (Å <sup>2</sup> )	<i>R</i> (Å)	$\sigma^2$ (Å <sup>2</sup> )
sample R1 (MnO <sub>4</sub> <sup>-</sup> /EDTA molar ratio 1)	1.90 ± 0.01	0.0051 ± 0.0004	2.85 ± 0.01	0.0087 ± 0.0005
sample R4 (MnO <sub>4</sub> <sup>-</sup> /EDTA molar ratio 4)	1.90 ± 0.01	0.0057 ± 0.0005	2.84 ± 0.01	0.0091 ± 0.0007

<sup>a</sup> Data of Mn K-edge EXAFS (CN for Mn–O = 6, Mn–Mn = 6).

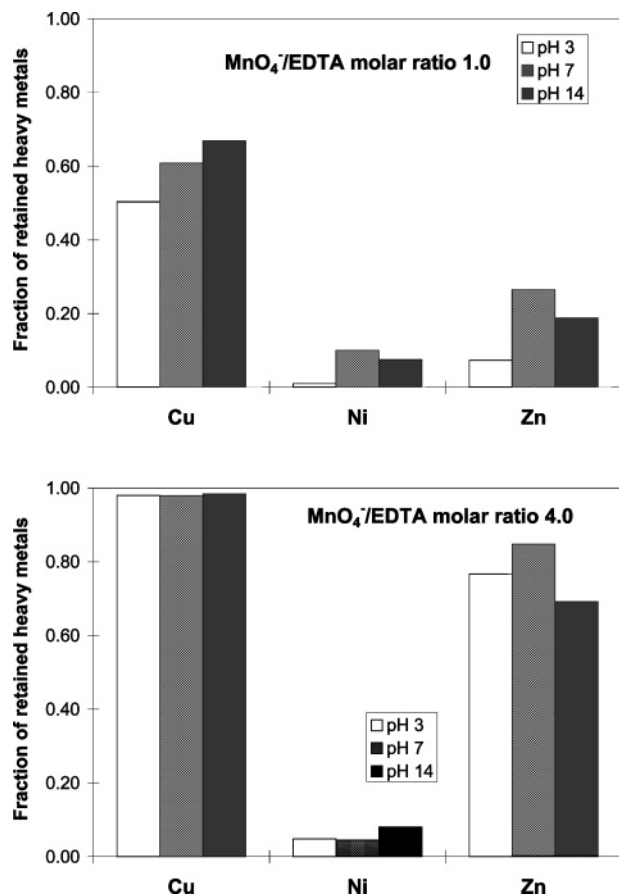


**FIGURE 2. Fraction of copper, nickel, and zinc retained by birnessite formed at pH 14 and washed at pH 14, 7, and 3. MnO<sub>4</sub><sup>-</sup>/EDTA ratios 1 and 4. Initial concentration of EDTA 0.02 M. Initial concentrations of copper, nickel, and zinc 0.002 M.**

structure (7). This arrangement is characteristic for phyllo-manganese minerals such as  $\delta$ -MnO<sub>2</sub> and birnessite (25–27). Based on the sum of the data of SEM, XRD, XANES, and EXAFS techniques, as well as results of prior research (7), we concluded that particles precipitated upon the oxidation of EDTA by permanganate are birnessite-type solids, although the presence of minor amounts of other Mn(IV) phases could not be ruled out completely.

Examination of the high-pH oxidation of EDTA by preformed MnO<sub>2</sub> showed that EDTA was stable in these conditions. It was accordingly concluded that reduction of Mn(IV) to Mn(III) by EDTA did not exceed the level defined by the precision of the experiments (5%). This indicates that the high-pH permanganate oxidation of EDTA is likely to result in the formation of low-sodium birnessite in which the charge deficit in the MnO<sub>6</sub> octahedra-comprised sheets is associated primarily with defects in the two-dimensional layers and lower charge cations such as Cu<sup>2+</sup> and Zn<sup>2+</sup> that are incorporated into them in statu nascendi, as described in the section that follows. The conclusion that low-sodium

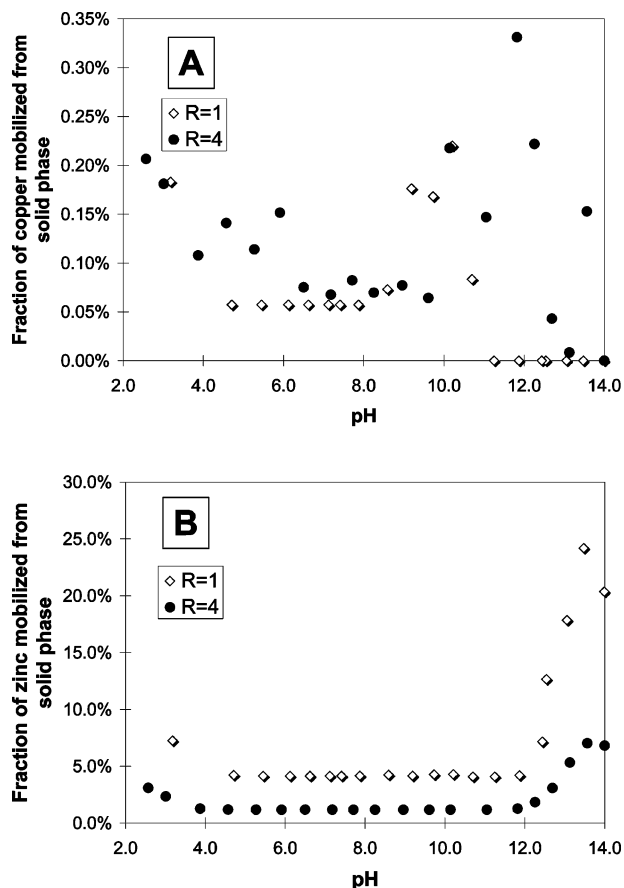


**FIGURE 3. Influence of pH on the fraction of copper (A) and zinc (B) released from suspended birnessite solids containing retained heavy metals.**

birnessite is formed upon the reduction of MnO<sub>4</sub><sup>-</sup> by EDTA is different from that obtained for the reduction of MnO<sub>4</sub><sup>-</sup> by stronger reduction agents such as H<sub>2</sub>O<sub>2</sub> and formate (7). In that case, the precipitated solids were ascribed the stoichiometry of the mineral clinobirnessite Na<sub>4</sub>Mn<sub>14</sub>O<sub>27</sub>·9H<sub>2</sub>O. Despite possible differences in the stoichiometries of the solid phases formed via the high-pH reduction of permanganate by EDTA or H<sub>2</sub>O<sub>2</sub>/formate, in either case the solids have phyllo-manganese-type structures (19).

Precipitation of birnessite particles was accompanied by effective removal of Cu<sup>2+</sup> and Zn<sup>2+</sup> that were present in the original solution as EDTA complexes (Figure 2). For a 1.0 MnO<sub>4</sub><sup>-</sup>/EDTA molar ratio, 60% and 18% of Cu and Zn, respectively, were retained by birnessite formed during the reaction. At a 4.0 MnO<sub>4</sub><sup>-</sup>/EDTA molar ratio, 98% and 77% of Cu and Zn, respectively, were removed. In contrast with that, the removal of nickel did not exceed 6% at all conditions. This was a result of the resistance of Ni<sup>2+</sup>-EDTA complexes toward oxidation (28, 29) and possibly lack of sorption of Ni<sup>2+</sup>-EDTA complexes on birnessite. The resistance of the Ni<sup>2+</sup>-EDTA complex during the high-pH permanganate

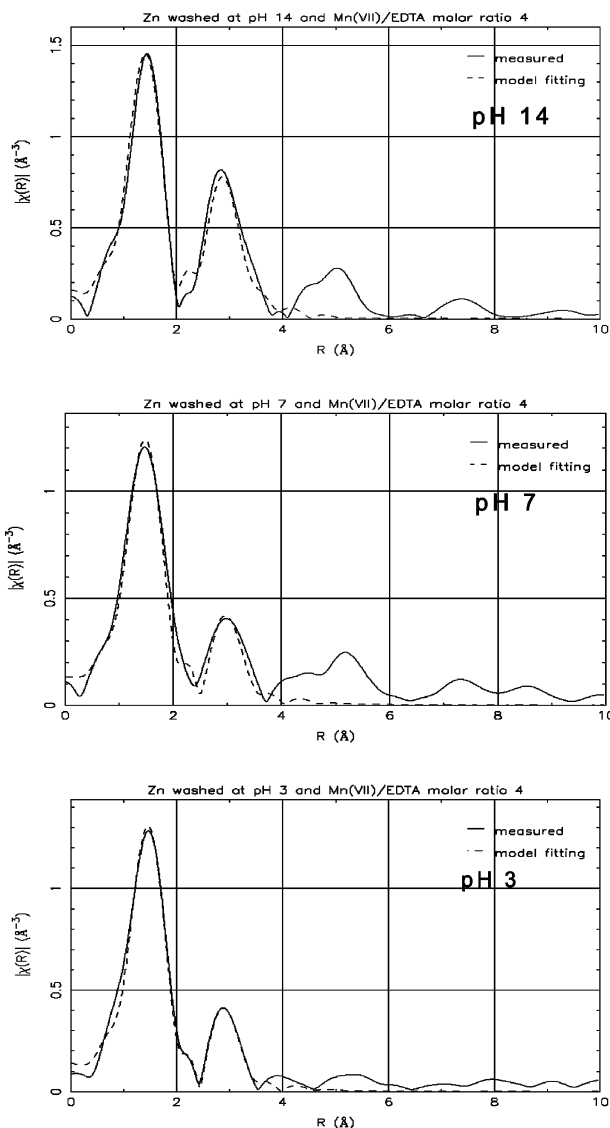


**FIGURE 4.** Comparison of experimental radial density functions and fitting results for  $\text{Zn}^{2+}$  retained by birnessite and washed at pH 14, 7, and 3.  $\text{MnO}_4^-/\text{EDTA}$  molar ratio 4.

treatment is not necessarily a result of a uniquely high thermodynamic stability of  $\text{Ni}^{2+}$ -EDTA complexes. In fact, the  $\log \beta$  values for  $\text{Cu}^{2+}$ -EDTA and  $\text{Ni}^{2+}$ -EDTA complexes are close, 20.5 and 20.1, respectively (28, 29), while the behavior of these metals is different. It can be hypothesized that the permanganate oxidation of  $\text{Ni}^{2+}$ -EDTA targets not only EDTA but also  $\text{Ni}^{2+}$  to produce  $\text{Ni}^{3+}$  that forms highly stable complexes with EDTA (28). Further exploration of this issue goes beyond the scope of this paper.

Washing at pH 7 and 3 caused a small fraction of copper bound by the solids formed using a 1.0  $\text{MnO}_4^-/\text{EDTA}$  molar ratio to be leached out (Figure 2). For solids formed using a 4.0  $\text{MnO}_4^-/\text{EDTA}$  molar ratio, the amount of copper bound in the solid phase was as stable at pH 3 as it was at pH 14. Results for zinc showed some variability, but increasing the  $\text{MnO}_4^-/\text{EDTA}$  molar ratio helped increase both the retention of this metal at pH 14 and its stability at lower pH. Despite the low efficiency of nickel removal during the permanganate oxidation, the amount of nickel that was bound by birnessite was stable during washing at pH 3 and 7 (Figure 2).

Experiments in which the pH of the suspensions was decreased from 14 to 3 showed that virtually no manganese release took place, but the retained  $\text{Zn}^{2+}$  and  $\text{Cu}^{2+}$  cations were mobilized to some extent, with systematic differences

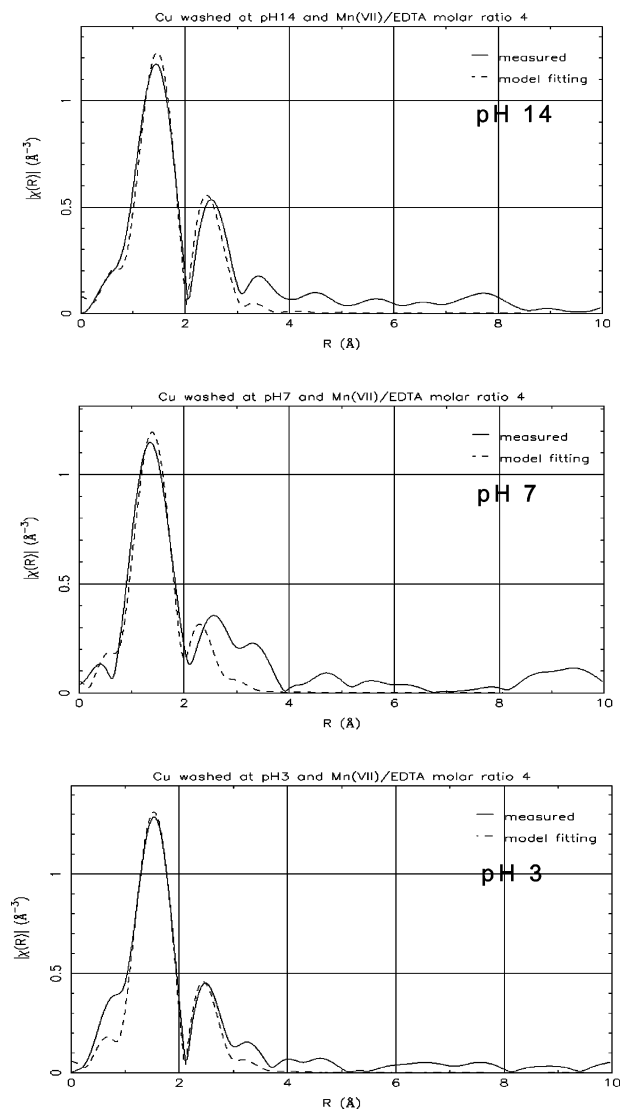


**FIGURE 5.** Comparison of experimental radial density functions and fitting results for  $\text{Cu}^{2+}$  retained by birnessite and washed at pH 14, 7, and 3.  $\text{MnO}_4^-/\text{EDTA}$  molar ratio 4.

between the behavior of copper and zinc. The copper retained by the particles formed using both 1 and 4  $\text{MnO}_4^-/\text{EDTA}$  molar ratios was stable in the entire range of pH values. Only about 0.2% of it was released into the supernatant at  $\text{pH} > 10$  (Figure 3A). At  $\text{pH} < 6$ , Cu release increased as well but even at pH 3 the percentage of copper mobilized from the solid phase did not exceed 0.2%.

Release of Zn was more prominent. For solids formed using a 1.0  $\text{MnO}_4^-/\text{EDTA}$  molar ratio, up to 25% of the zinc initially retained by birnessite was released at  $\text{pH} > 12$  (Figure 3B). The mobility of zinc also slightly increased at  $\text{pH} < 4$ . A similar pattern was observed for solids formed using a 4.0  $\text{MnO}_4^-/\text{EDTA}$  molar ratio, but the amount of zinc in contact with it decreased more than 3-fold.

To probe mechanisms that govern the retention of  $\text{Zn}^{2+}$  and  $\text{Cu}^{2+}$  by in situ formed birnessite, EXAFS measurements for Cu and Zn were performed. The concentrations of Zn and Cu in the samples are shown in Figure S4 in the Supporting Information. EXAFS measurements for Ni were not carried out.

The analysis of the Zn EXAFS data was initially done assuming that the immobilized  $\text{Zn}^{2+}$  was bound at the defect sites located in the layers formed by  $\text{MnO}_6$  octahedra. However, it was observed that the Zn-Mn distance that was

**TABLE 2. Structural Characteristics of Zinc in Solids Formed via the Oxidation of EDTA by Permanganate at pH 14<sup>a</sup>**

sample	Zn–O		Zn–Mn	
	<i>R</i> (Å)	$\sigma^2$ (Å <sup>2</sup> )	<i>R</i> (Å)	$\sigma^2$ (Å <sup>2</sup> )
sample R1, pH 14	1.93 ± 0.02	0.010 ± 0.002	3.34 ± 0.04	0.006 ± 0.002
sample R1, pH 7	1.97 ± 0.01	0.011 ± 0.001	3.40 ± 0.03	0.013 ± 0.002
sample R1, pH 3	1.91 ± 0.02	0.009 ± 0.002	3.30 ± 0.05	0.010 ± 0.003
sample R4, pH 14	1.94 ± 0.02	0.010 ± 0.002	3.35 ± 0.05	0.006 ± 0.002
sample R4, pH 7	2.01 ± 0.02	0.012 ± 0.002	3.44 ± 0.05	0.015 ± 0.004
sample R4, pH 3	1.99 ± 0.01	0.011 ± 0.002	3.37 ± 0.02	0.016 ± 0.002

<sup>a</sup> Data of Zn K-edge EXAFS (CN for Zn–O = 6, Zn–Mn = 6).

**TABLE 3. Structural Characteristics of Copper in Solids Formed via the Oxidation of EDTA by Permanganate at pH 14<sup>a</sup>**

sample	equatorial Cu–O (4)		axial Cu–O (2)		Cu–Mn (6)	
	<i>R</i> (Å)	$\sigma^2$ (Å <sup>2</sup> )	<i>R</i> (Å)	$\sigma^2$ (Å <sup>2</sup> )	<i>R</i> (Å)	$\sigma^2$ (Å <sup>2</sup> )
sample R1, pH 14	1.95 ± 0.08	0.007 ± 0.008	1.97 ± 0.08	0.007 ± 0.008	2.85 ± 0.08	0.021 ± 0.009
sample R1, pH 7	1.93 ± 0.06	0.005 ± 0.008	1.98 ± 0.08	0.005 ± 0.008	2.84 ± 0.08	0.025 ± 0.010
sample R1, pH 3	1.91 ± 0.03	0.002 ± 0.009	2.00 ± 0.09	0.002 ± 0.009	2.81 ± 0.09	0.031 ± 0.014
sample R4, pH 14	1.93 ± 0.04	0.004 ± 0.004	2.01 ± 0.08	0.004 ± 0.004	2.89 ± 0.08	0.018 ± 0.005
sample R4, pH 7	1.89 ± 0.05	0.001 ± 0.011	2.02 ± 0.13	0.001 ± 0.011	2.80 ± 0.13	0.035 ± 0.029
sample R4, pH 3	2.00 ± 0.03	0.004 ± 0.004	1.99 ± 0.13	0.004 ± 0.004	2.87 ± 0.13	0.022 ± 0.009

<sup>a</sup> Data of Cu K-edge EXAFS (CN for Cu–O = 6, including 4 equatorial and 2 axial bonds; Cu–Mn = 6).

assumed to exist for this structure was inconsistent with the observations. Because of that, the local structure around the Zn<sup>2+</sup> ions was hypothesized to be similar to that of chalcophanite ZnMn<sub>3</sub>O<sub>7</sub>·3H<sub>2</sub>O. The structure of chalcophanite is formed by sheets of layered MnO<sub>6</sub> octahedra with one vacant site per every seven cation sites. The Zn<sup>2+</sup> ions are coordinated in chalcophanite above the vacant sites located in the sheets of MnO<sub>6</sub> octahedra (12, 30).

Processing of the Zn EXAFS data using this hypothesis resulted in an acceptable level of goodness-of-fit. The results for pH 3, 7, and 14 for a 4.0 MnO<sub>4</sub><sup>−</sup>/EDTA ratio are shown in Figure 4. Additional Zn EXAFS data for solids formed at a 1.0 MnO<sub>4</sub><sup>−</sup>/EDTA ratio are represented in Figure S5 in the Supporting Information.

The information obtained based on Zn EXAFS data is summarized in Table 2. The data show that the average Zn–O and Zn–Mn distances in all samples are close, with two trends related to the effects of pH and MnO<sub>4</sub><sup>−</sup>/EDTA dose. First, the Zn–O and Zn–Mn distances at pH 7 (2.01 and 3.44 Å respectively for a 4.0 MnO<sub>4</sub><sup>−</sup>/EDTA ratio) are somewhat longer than those for pH 3 and 14. Second, these distances are slightly longer in the samples obtained using a 4.0 MnO<sub>4</sub><sup>−</sup>/EDTA molar ratio. The values of the Debye–Waller factor ( $\sigma^2$ ) indicating the disorder of the Zn–O bonds are similar for all conditions, while those for the Zn–Mn distances are somewhat lower at pH 14.

Despite these changes, the local structure around the Zn<sup>2+</sup> ions immobilized in the birnessite particles remains similar to that of chalcophanite in all cases. It is likely that during the in situ formation of the birnessite, their structure undergoes a change induced by interactions with the decomplexed Zn<sup>2+</sup> to produce, locally, chalcophanite-type structures for sites at which Zn<sup>2+</sup> is incorporated. This is in agreement with the data of prior studies of the incorporation of Zn<sup>2+</sup> into preformed birnessite (13, 15).

Attempts to fit the Cu EXAFS data assuming a structural arrangement similar to that of chalcophanite were unsuccessful. Accordingly, it was hypothesized that Cu<sup>2+</sup> was bound at sites located within the two-dimensional sheets comprised by MnO<sub>6</sub> octahedra. It was also assumed that the number of nearest neighbors in the inner shell of the bound Cu<sup>2+</sup> ions was six, including four equatorially and two axially positioned oxygen atoms with potentially different Cu–O distances

(Jahn–Teller effect) (15, 22, 31–33). The number of manganese atoms that affect the EXAFS spectra of incorporated Cu<sup>2+</sup> ions was six.

This hypothesis allowed obtaining a good quality of fitting for the Cu EXAFS data. Figure 5 compares the results of the fitting that utilized these assumptions and experimental Cu EXAFS data for the sample generated using a 4.0 MnO<sub>4</sub><sup>−</sup>/EDTA ratio. Additional Cu EXAFS data for solids formed at a 1.0 MnO<sub>4</sub><sup>−</sup>/EDTA ratio are represented in Figure S6 in the Supporting Information. The structural data for Cu<sup>2+</sup> bound in birnessite are summarized in Table 3. They indicate that neither the pH of the washing solution nor MnO<sub>4</sub><sup>−</sup>/EDTA molar ratio at which these solids were formed affects the structural status of the bound copper. The equatorial Cu–O distances (ca. 1.89–1.95 Å, except one sample washed at pH 3, Table 3) determined for all samples are close to those determined for equatorially bound oxygen atoms in aqueous Cu<sup>2+</sup> complexes and many sorbed Cu<sup>2+</sup> species (15, 22, 31–33). Both the axial Cu–O distances for Cu<sup>2+</sup> incorporated into birnessite (1.97–2.02 Å) and their respective Debye–Waller factors are close to those for the equatorial bonds. This indicates a nearly complete elimination of the Jahn–Teller effect. This is indicative of strong interactions between the incorporated Cu<sup>2+</sup> ions and MnO<sub>6</sub> octahedra that surround them.

The Debye–Waller factors for the Cu–Mn distances are higher than those for the Cu–O bonds, and the scatter of the Cu–Mn distances exhibit an increase when the pH is decreased from 14 to 3 (Table 3). This is likely to indicate that although Cu<sup>2+</sup> remains tightly bound in the birnessite at pH values as low as 3, the strength of bonds between this metal and the substrate becomes weaker.

The Cu–Mn distances in all samples are similar (2.80–2.89 Å). This value is close to that for the Mn–Mn distance (2.85 Å) in unsubstituted birnessite (Table 1). This provides a strong indication that that little distortion of the layers formed by MnO<sub>6</sub> octahedra takes place when Cu<sup>2+</sup> is incorporated into them.

The above structural data indicate that the birnessite-type solids formed during the oxidation of high-pH, high-ionic nuclear wastes containing EDTA and similar organic ligands are likely to resist mobilization of heavy metals such as Cu and Zn incorporated into them in a wide range of

environmental conditions, as long as the reduction of Mn(IV) that predominates in the solid is prevented. The issue of whether the representative TRU is bound in a manner similar to that established in this study for Zn<sup>2+</sup> and Cu<sup>2+</sup> needs further exploration.

### Acknowledgments

This study was supported by Consortium for Risk Evaluation and Stakeholder Participation (CRESP), Department of Energy Grant DE FG01-03EW1536. A.I.F. acknowledges support by the U.S. Department of Energy Grant No. DE-FG02-03ER15477. NSLS is supported by the Divisions of Materials and Chemical Sciences of DOE. The views represented in this publication do not necessarily represent those of the funding agencies.

### Supporting Information Available

Six figures demonstrating changes of the specific surface area of birnessite solids precipitated during the reduction of permanganate by EDTA at varying reaction times, the morphology of these solids and their Mn XANES spectra, and concentrations of and EXAFS radial density functions for Cu and Zn retained by birnessite formed using a low permanganate/EDTA molar ratio. This material is available free of charge via the Internet at <http://pubs.acs.org>.

### Literature Cited

- U.S. Environmental Protection Agency. *In situ remediation technology: in situ chemical oxidation*; EPA 542-R-98-008; Office of Solid Waste and Emergency Response, U.S. EPA: Washington DC, 1998.
- Siegrist, R. L.; Urynowicz, M. A.; West, O. R.; Crimi, M. L.; Lowe, K. S. *Principles and practices of in situ chemical oxidation using permanganate*; Battelle Press: Columbus, OH, 2001.
- Hallen, R. T.; Geeting, J. G. H.; Lilga, M. A.; Hart, T. R.; Hoopes, F. V. Assessment of the mechanisms for Sr-90 and TRU removal from complexant-containing tank wastes at Hanford. *Sep. Sci. Technol.* **2005**, *40* (1), 171–183.
- Chang, H. S.; Korshin, G. V.; Ferguson, J. F. Examination of reaction mechanisms and reaction products for the oxidation of EDTA by permanganate at high pH values. *Environ. Sci. Technol.* **2006**, *40* (16), 5089–5094.
- Bond, A. H.; Nash, K. L.; Gelis, A. V.; Sullivan, J. C.; Jensen, M. P.; Rao, L. Plutonium mobilization and matrix dissolution during experimental sludge washing of bismuth phosphate, redox and purex waste simulants. *Sep. Sci. Technol.* **2001**, *36* (5/6), 1241–1256.
- Peters, T. B.; Fink, S. D.; Hobbs, D. T.; Norato, M. A.; Walker, D. D. *Demonstration of MST and Permanganate Efficiency on Removal of Actinides and Strontium from Savannah River Site High Level Waste*; Report WSRC-TR-2002-00355; Westinghouse Savannah River Company: Aiken, SC, 2003.
- Duff, M. C.; Hunter, D. B.; Hobbs, D. T.; Jurgensen, A.; Fink, S. D. *Characterization of Plutonium, Neptunium, Strontium on Manganese Solids from Permanganate Reduction*; Report WSRC-TR-2002-00366; Westinghouse Savannah River Company: Aiken, SC, 2002.
- Taylor, R. M.; McKenzie, R. M.; Fordham, A. W.; Gillman, G. P. Oxide minerals. *Soils: An Australian Viewpoint*; Academic Press, CSIRO: London, 1983.
- Huang, P. M. Kinetics of redox reactions on manganese oxides and its impact on environmental quality. *Rates of Soil Chemical Processes*; Soil Science Society of America: Madison, WI, 1991; pp 191–230.
- Dixon, J. B.; Skinner, H. C. W. Manganese minerals in surface environments. *Biomining processes of Iron and Manganese: Modern and Ancient Environments*; CATENA Verlag: Reiskirchen, Germany, 1992; pp 31–50.
- Stouff, P.; Boulegue, J. Synthetic 10-Å and 7-Å phyllosulfates: Their structures as determined by EXAFS. *Am. Mineral.* **1988**, *73* (9/10), 1162–1169.
- Post, J. E.; Appleman, D. E. Chalcophanite ZnMn<sub>3</sub>O<sub>7</sub>·3H<sub>2</sub>O: New crystal-structure determinations. *Am. Mineral.* **1988**, *73* (11/12), 1401–1404.

- Silvester, E.; Manceau, A.; Drits, V. A. Structure of synthetic monoclinic Na-rich birnessite and hexagonal birnessite: II. Results from chemical studies and EXAFS spectroscopy. *Am. Mineral.* **1997**, *82* (9/10), 962–978.
- Post, J. E. Manganese oxide minerals: Crystal structures and economic and environmental significance. *Proc. Natl. Acad. Sci. U.S.A.* **1999**, *96* (7), 3447–3454.
- Manceau, A.; Lanson, B.; Drits, V. A. Structure of heavy metal sorbed birnessite. Part III: Results from powder and polarized extended X-ray absorption fine structure spectroscopy. *Geochim. Cosmochim. Acta* **2002**, *66* (15), 2639–2663.
- Zabinsky, S. I.; Rehr, J. J.; Ankudinov, A.; Albers, R. C.; Eller, M. J. Multiple-scattering calculations of x-ray absorption spectra. *Phys. Rev. B* **1995**, *52* (4), 2995–3009.
- Crimi, M. L.; Siegrist, R. L. Impact of Reaction Conditions on MnO<sub>2</sub> Genesis during permanganate oxidation. *J. Environ. Eng.* **2004**, *130* (5), 562–572.
- Powder Diffraction File. Alphabetical Index. Inorganic Phases*; International Center for Diffraction Data: Swarthmore, PA, 1988.
- Gaillot, A. C.; Drits, V. A.; Manceau, A.; Lanson, B. Structure of the synthetic K-rich phyllosulfate birnessite obtained by high-temperature decomposition of KMnO<sub>4</sub>. Substructures of K-rich birnessite from 1000 °C. *Microporous Mesoporous Mater.* **2007**, *98*, 267–282.
- Jokic, A.; Frenkel, A. I.; Vairavamurthy, M.; Huang, P. M. Birnessite catalysis of the Maillard reaction: Its significance in natural humification. *Geophys. Res. Lett.* **2001**, *28* (20), 3899–3902.
- Jokic, A.; Wang, M. C.; Liu, C.; Frenkel, A. I.; Huang, P. M. Integration of the polyphenol and Maillard reactions into unified abiotic pathway for humification in nature: the role of δ-MnO<sub>2</sub>. *Org. Geochem.* **2004**, *35* (6), 747–762.
- Manceau, A.; Gorshkov, A. I.; Drits, V. A. Structural chemistry of Mn, Fe, Co, and Ni in manganese hydrous oxides: Part I. Information from XANES spectroscopy. *Am. Mineral.* **1992**, *77* (11/12), 1133–1143.
- Villinski, J. E.; O'Day, P. A.; Corley, T. L.; Conklin, M. H. In situ spectroscopic and solution analyses of the reductive dissolution of MnO<sub>2</sub> by Fe(II). *Environ. Sci. Technol.* **2001**, *35* (6), 1157–1163.
- Fredrickson, J. K.; Zachara, J. M.; Kennedy, D. W.; Liu, C.; Duff, M. C.; Hunter, D. B.; Dohnalkova, A. Influence of Mn oxides on the reduction of U(VI) by the metal-reducing bacterium. *Shewanella putrefaciens*. *Geochim. Cosmochim. Acta* **2002**, *66* (18), 3247–3262.
- Post, J. E.; Veblen, D. R. Crystal structure determinations of synthetic sodium, magnesium, and potassium birnessite using TEM and the Rietveld method. *Am. Mineral.* **1990**, *75* (5/6), 477–489.
- Giovanoli, R.; Stahli, E.; Feitknecht, W. Über Oxidhydroxide des vierwertigen Mangans mit Schichtengitter I. Mitteilung: Natriummangan (II,III) Manganat (IV). *Helv. Chim. Acta* **1970**, *53* (2), 209–220.
- Chukhrov, F. V.; Sakharov, B. A.; Gorshkov, A. I.; Drits, V. A.; Dikov, Y. P. The structure of birnessite from the Pacific Ocean. *Izv. Akad. Nauk SSSR, Ser. Geol.* **1985**, *8*, 66–73.
- Mandal, P. C.; Bardhan, D. K.; Sarkar, S.; Bhattacharyya, S. N. Oxidation of nickel (II) ethylenediaminetetraacetate by carbonate radical. *J. Chem. Soc., Dalton Trans.* **1991**, *6*, 1457–1461.
- Felmy, A. R.; Qafoku, O. An aqueous thermodynamic model for the complexation of nickel with EDTA valid to high base concentrations. *J. Solution Chem.* **2004**, *33* (9), 1161–1180.
- Wadsley, A. D. The crystal structure of chalcophanite, ZnMn<sub>3</sub>O<sub>7</sub>·3H<sub>2</sub>O. *Acta Crystallogr.* **1955**, *8*, 165–172.
- Palladino, L.; Della Longa, S.; Reale, A.; Belli, M.; Scafatti, S.; Onori, G.; Santucci, A. X-ray absorption near edge structure (XANES) of Cu(II)-ATP and related compounds in solution: quantitative determination of the distortion of the Cu site. *J. Chem. Phys.* **1993**, *98* (4), 2720–2726.
- Douglas, B.; McDaniel, D.; Alexander, J. *Concepts and Models of Inorganic Chemistry*; Wiley: New York, 1994.
- Korshin, G. V.; Frenkel, A. I.; Stern, E. A. EXAFS study of the inner shell structure in copper (II) complexes with humic substances. *Environ. Sci. Technol.* **1998**, *32* (18), 2699–2705.

Received for review October 24, 2006. Revised manuscript received January 20, 2007. Accepted January 22, 2007.

ES062554T